Journal of Geophysical Research: Atmospheres

Supporting Information for

More than emissions and chemistry: Fire size, dilution, and background aerosol also greatly influence near-field biomass burning aerosol aging

A. L. Hodshire[1], Q. Bian[1], E. Ramnarine[1], C. R. Lonsdale[2], M. J. Alvarado[2], S. M. Kreidenweis[1], S. H. Jathar[3], J. R. Pierce

[1]Department of Atmospheric Science, Colorado State University, Fort Collins, CO, USA, [2]Atmospheric and Environmental Research, Inc., Lexington, Massachusetts, USA, [3]Department of Mechanical Engineering, Colorado State University, Fort Collins, CO, USA

Contents of this file

Text S1 to S6
Figures S1 to S24
Table S1

Additional Supporting Information (Files uploaded separately)

Captions for Tables S2

Introduction

The following provides addition model results, including results for all fire sizes and background aerosol concentrations modelled (see text section S1; Figs. S1, S2, S5, S9, and S11) and the results of all sensitivity analyses done in the study (text section S5; Figs. S13-S24). We detail our modeling smoothing techniques in text section S2, provide the calculations for the plume mean diameter and peak lognormal modal width. Text section S3 details a discussion on the formation of SOA and role of condensing vapor volatility on plume mean diameter and peak lognormal modal width and CCN concentrations. Finally, table S1 (loaded separately) provides a brief overview of published biomass burning field campaings, in the context of this study.

Text S1. Additional model results

Figures S1 shows the time evolution of smoke organic mass enhancement (ΔOA) and dilution ratios for the base simulations all fire sizes and background concentrations modelled in this study. Figure S2 shows the time evolution of ΔCO for a subset of the fire sizes. ΔCO is not impacted by background aerosol concentration or the aerosol chemistry and coagulation model schemes. Figure S3 shows ΔOA normalized by the enhancement of CO above background (ΔCO) after four hours of aging for all combinations of Chem and Coag simulations for all fire sizes and background concentrations modelled for the base simulations. Figures S4-S5 give the initial and final volatility basis set (VBS) distributions for the base simulations for background aerosol concentrations of 5 and 50 μg m^{-3}, respectively. The k_{OH} from the Jathar et al. (2014) parameterization is sufficiently slow at high C* values that only a small fraction of the highest volatility bins (~C* ≥ 10^6 μg m^{-3}) undergo oxidative aging within the 4 simulated hours, thus contributing little to final normalized smoke OA. Figure S6 provides ΔOA/ΔCO for the base cases as a function of time for all fire sizes and background concentrations modelled. Shown are the ChemOn_CoagOn and ChemOff_CoagOff cases (as coagulation does not change the total mass significantly). Figure S7 provides the background corrected lognormal diameter, D_g, and lognormal modal width, σ_g, for all background concentrations and fire sizes between 10^{-2} and 100 km^2 for the base cases modelled in this study after 4 hours of aging. Figures S8 and S9 provide the number and volume size distributions for the base cases (Table 1) after 4 hours of aging for a subset of the fire sizes (10^{-2}, 1, and 100 km^2) and background aerosol concentrations (0, 5, and 50 μg m^{-3}). We show the total (plume plus background aerosol) size distributions, as well as the background alone size distributions. Figure S10 provides $\Delta E/\Delta$CO for the base cases after 4 hours of aging for all background aerosol concentrations and fire sizes between 10^{-2} and 100 km^2. Figure S11 shows the size-dependent mass extinction efficiency for the refractive index used in this study, 1.5 - 0.08i (assuming spherical particles) at a wavelength of 500 nm. Figure S12 provides ΔCCN/ΔCO at 0.2% supersaturation for the base cases after 4 hours of aging for all background aerosol concentrations and fire sizes between 10^{-2} and 100 km^2. It is assumed that both the plume and background aerosol have hygroscopicity parameter (κ) values of 0.2.

Text S2. Model smoothing

In TOMAS, we use a top hat method for transferring mass between size sections during condensation/evaporation, as described in Stevens et al. (1996). First a top hat representation of the distribution is constructed for each bin, then these are translated according to the analytic solution, and then finally the translated top hats are remapped to the bins. However, in the tophat method, at times a bin will empty out into an adjacent largest bin, creating oscillations of number/mass within the diameter space. To reduce the noise created by these oscillations during post processing, we transfer mass between adjacent bins in post-processing by moving number to make the mass:number ratio in each bin equal to the geometric mean of the bin mass:number limits. This method conserves total number and mass.

When the fire size distribution is very close to the background size distribution (relevant for fires 10^{-2} km^2 and smaller in this work), the post-processing smoothing of the total size

distributions (plume and background) occasionally does not line up with the background-only simulations well enough and poor results are obtained. The following results have been skewed by model noise and are removed from this study:

- The base simulation: The plume peak diameter of the lognormal mode and and lognormal modal width data point for the ChemOff_CoagOn case for the 10^{-2} km^2 fire with a 20 μg m^{-3} background (Fig. S7)
- The sensitivity case of a stability class of B: the smoke extinction data point for the ChemOn_CoagOff case's value for E_{smoke} for the 10^{-2} fire size with a 50 μg m^{-3} background concentration (Fig. S19)

Text S3. Calculations of the plume geometric mean diameter and peak lognormal modal width

Whitby et al. (1991) determined mathematical relationships between integral moments M_k and the geometric mean diameter (D_g) and peak lognormal modal width (σ_g,) for integer values of k_1 and k_2:

$$D_g = \overline{M}_{k_1}^{\hat{k}_1} \overline{M}_{k_2}^{\hat{k}_2} \qquad (1)$$

$$ln^2(\sigma_g) = \frac{2}{k_1(k_1 - k_2)} ln(\frac{\overline{M}_{k_1}}{\overline{M}_{k_2}^{r}}) \qquad (2)$$

where $\overline{M}_k = M_k/N$, $r = k_1/k_2$, $\hat{k}_1 = 1/[r(k_2 - k_1)]$, $\hat{k}_2 = r/(k_1 - k_2)$, and N is the total number concentration. We use each combination of integral moments 1, 2, 3, and 4 for k_1 and k_2 and present the average of each moment combination for D_g and σ_g. (Note that k_1 cannot equal k_2).

Text S4. Discussion of the impact of volatility-dependent SOA formation on plume σ_g, D_g, and CCN

The size-dependent growth/shrink rates during condensation/evaporation is controlled by two different processes: the volatilities of the condensing vapors and the sizes of the growing particles (in the absence of particle-phase diffusion effects and significant differences in composition with size). For condensation, if the condensing species have a low-enough effective volatility (an effective saturation concentration $C^* <\sim 10^{-3}$ μg m^{-3}), the vapors will condense essentially irreversibly (Pierce et al., 2011; Riipinen et al., 2011; Zhang et al., 2012). Under irreversible condensation, growth rates are independent of D_p in the kinetic regime (particles smaller than ~50 nm) but proportional to $1/D_p$ in the continuum regime (particles greater than ~1 μm; Seinfeld & Pandis, 2006). As a result, irreversible condensation will grow smaller particles more quickly than larger particles in the continuum regime. This effect is seen for the smallest fires in the ChemOff cases (Figs. 3 and S6): σ_g increases slightly for these cases, indicating that dilution and evaporation rates are great enough that some of the lower-volatility material is also evaporating off, broadening the distribution. Conversely, if the vapors are instead semivolatile ($C^* >\sim 10^{-1}$ μg m^{-3}), vapors will more quickly reach equilibrium at all particle sizes and growth will be in quasi-equilibrium, which is proportional to particle diameter (D_p) for all particle sizes (Pierce et al., 2011; Riipinen et al., 2011; Zhang et al., 2012). Thus, if only semivolatile vapors were condensing (evaporating) in the plume, σ_g would not decrease (increase). This effect can be seen for most fire sizes in the ChemOff cases in which evaporation of semi-volatile

compounds decreases the mean diameter, D_g, but the lognormal modal width, σ_g, remains essentially constant (Figs. 3 and S7).

The majority of the simulated plume particles are in the transition and continuum regimes (Fig. S8). In the transition regime, irreversible condensation growth rates will transition in between having no D_p dependence to having a $1/D_p$ dependence (Seinfeld & Pandis, 2006), while quasi-equilibrium condensation always has a D_p dependence. For the ChemOn cases, where SOA is being produced through gas-phase chemistry, σ_g generally decreases in the cases where SOA production dominates (Figs. 3 and S7), which indicates that this SOA condensation is occuring closer to the irreversible limit than the quasi-equilibrium limit. It is of note that for the smaller fire sizes (area 0.1 km^2 and smaller), increasing background concentrations leads to less of a total decrease in σ_g in our simulations, as more low volatility vapors are able to condense onto the smoke aerosol (OA evaporation decreases with higher background concentrations as the increased mass from the background aerosol drives partitioning to the aerosol phase; Donahue et al., 2006). Thus, the D_p dependence on growth rates for small fire sizes with higher background concentrations is shifted more towards a proportionality in D_p (quasi-equilibrium) than in $1/D_p$ (irreversible) for the transition and continuum regime-sized particles.
The effects of the irreversible and quasi-equilibrium condensation on D_g discussed above also impact D_g, which in turn impacts CCN concentrations. Figures 4 and S7 shows that for the smaller fires, SOA production (moving from chem_off to chem_on simulations) increases D_g while decreasing σ_g as the growth is primarily irreversible. However, for the smallest fires at the lowest background concentrations, evaporation of semi-volatile compounds (initial to chem_off; decreases D_g with ~constant σ_g) competes with approximately irreversible condensation. The net effect is that D_g remains approximately constant, while σ_g has decreased. As a result, the aged size distribution becomes more narrow but has an approximately constant D_g for the smallest fires at the lowest background concentrations.

Text S5. Sensitivity tests: accommodation coefficient, rate of OH reactions, stability class

Figures 1-4 show the results of plume evolution for the base cases, which use an accommodation coefficient of 1.0, the upper-bound chemistry parameterization with a four-bin drop in volatility per reaction with OH, and an atmospheric stability class of D (neutral). Here we briefly discuss the results and main differences from the base cases and sensitivity cases using accommodation coefficients of 0.1 and 0.01, the lower-bound chemistry parameterization with a two-bin drop in volatility per reaction with OH, and atmospheric stability classes of B and F. Figures S12-S22 provide ΔOA/ΔCO, $\Delta E/\Delta$CO, ΔCCN/ΔCO, peak diameter (D_g), and lognormal modal width (σ_g) information for a subset of fire sizes (10^{-2}, 1, and 100 km^2) and background aerosol concentrations (0, 5, and 50 μg m^{-3}). We also provide these data for the base cases after 8 hours of aging (Figs S23-S24). The purpose of these cases is to provide an overview of expected shifts in smoke properties under varying chemical and atmospheric conditions as well as age. Note that all colorbars are held fixed to the colorbars used in the main text, expect for the 8 hours of aging figure.

As the accommodation coefficient α decreases (Figs. S9-S12), both the SOA mass uptake and evaporation rates decrease (Seinfeld & Pandis, 2006), leading to decreases in the total aged smoke mass, extinction cross section, and CCN for medium to small fires with low to moderate background aerosol concentrations for ChemOn cases; the largest fire modelled (100 km^2) is not significantly impacted by decreases in α due to the large condensation sink when the particles stay concentrated in the large plume. Decreasing the rate of chemical reactions by using the lower-bound chemistry simulations with a two-bin drop in volatility per reaction with OH (Figs. S17-S18) decreases the rate at which lower

volatility materials are formed, slowing SOA formation for all fire sizes. Fig. S18 (for D_g and σ_g) shows evidence that for the lower-bound chemistry simulations, when chemistry is on, the majority of the vapors that are oxidizing and condensing in the model are semivolatile, as σ_g does not decrease beyond the decrease caused by coagulation in the largest fire and only decreases slightly for the smaller fire sizes (as the growth rate of semivolatile vapors is proportional to particle diameter at all particle sizes; Sect S4).

Decreasing (increasing) the atmospheric stability increases (decreases) the rate of OA evaporation, as dilution rates will increase (decrease) with changing stability (Figs. S19-S22). Finally, extending the base cases from 4 to 8 hours (Figs. S23-S24) allows for more OA evaporation and SOA formation, leading to greater increases (ChemOn) or decreases (ChemOff) in smoke mass and E for all fire sizes and greater increases (ChemOn) in CCNfor fires small enough to not be impacted by coagulation.

While the aged normalized mass and extinction values tend to follow the trends seen for the base cases presented in the main text, the aged normalized CCN values are more variable. In general, the final ΔCCN/ΔCO values are quite sensitive to the relative increases in mass and decreases in σ_g as can be seen in the sensitivity cases (Figs. S13-S22). In cases that lead to smaller mass gains in the largest plumes (e.g. for the lower-bound chemistry assumption) or more stable atmospheric conditions (leading to slower dilution rates; the sensitivity case of a stability class of F), ΔCCN/ΔCO tends to decrease below the initial ΔCCN/ΔCO values in the largest fires, as coagulational losses exceed gains from diameter growth from SOA production (Figs. S15, S17, S21).

Text S6. Biomass burning field campaings

Table S1 (uploaded separately as an excel file) details many publications on biomass burning field studies that focused on the aging plume. This table is not intended to be a comprehensive overview of biomass burning studies but instead a large sampling of relevant work. Table S1 is organized alphabetically by campaign name and then first author (for studies not associated with named field campaigns).

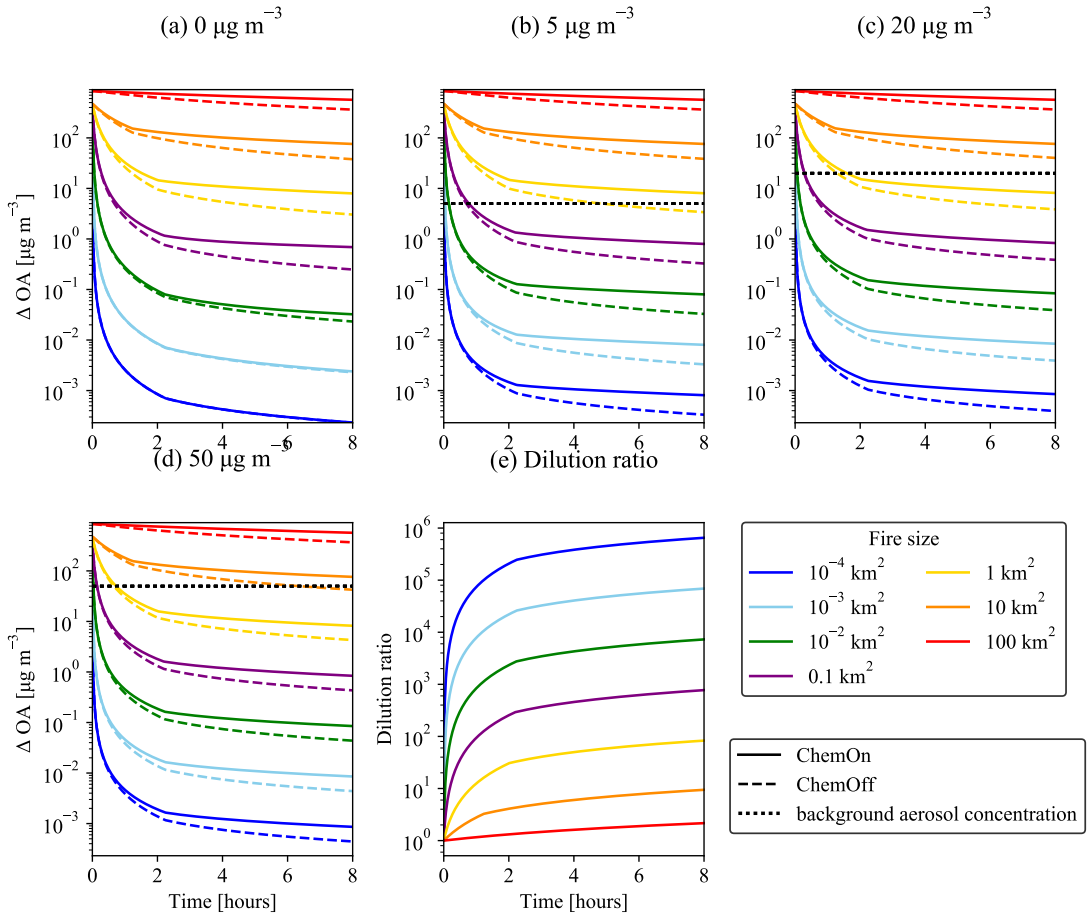

Figure S1. (a)-(d) Time evolution of total smoke organic aerosol mass concentration enhancement (background organic aerosol subtracted off) in the particle phase for chemistry-on (solid lines) and chemistry-off (dashed lines) simulations for the fire areas of 10^{-4}, 10^{-2}, 1, and 100 km^2 (colored lines) and background aerosol concentrations (black dashed lines) of (a) 0, (b) 5 μg m^{-3}, (c) 20 μg m^{-3}, and (d) 50 μg m^{-1}. (e) Time evolution of the dilution ratio for each fire size. Results are for the base simulations (Table 1) from the CoagOn version of each ChemOff/ChemOn case.

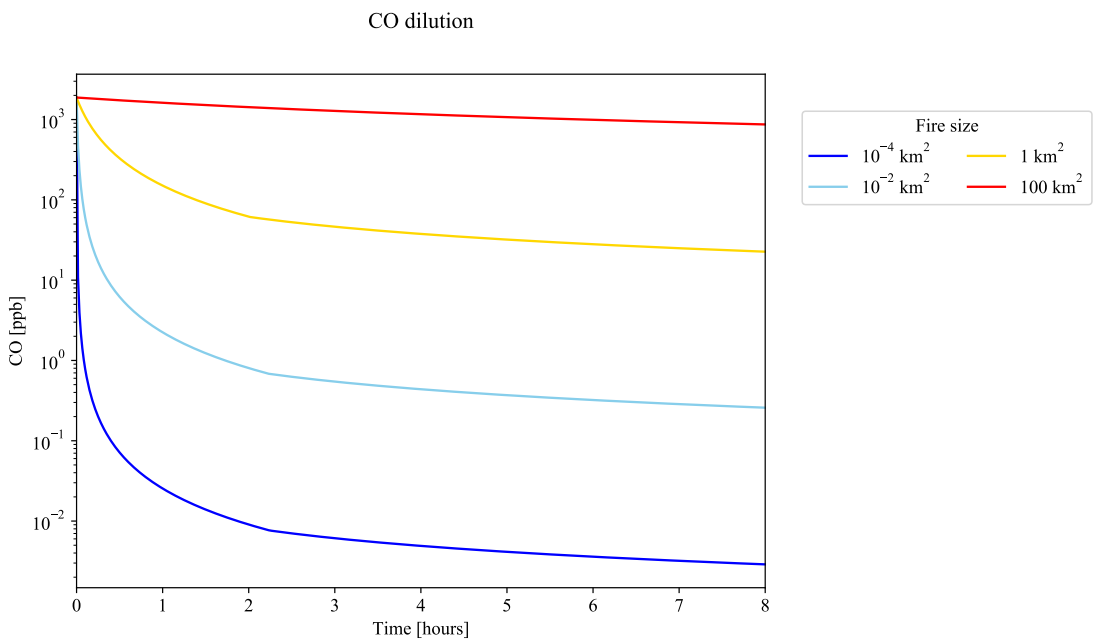

Figure S2. ΔCO dilution for each primary fire size for 8 hours of aging, using the assumptions of the base simulations (Table 1). ΔCO is not impacted by background aerosol concentration or the aerosol chemistry and coagulation model schemes.

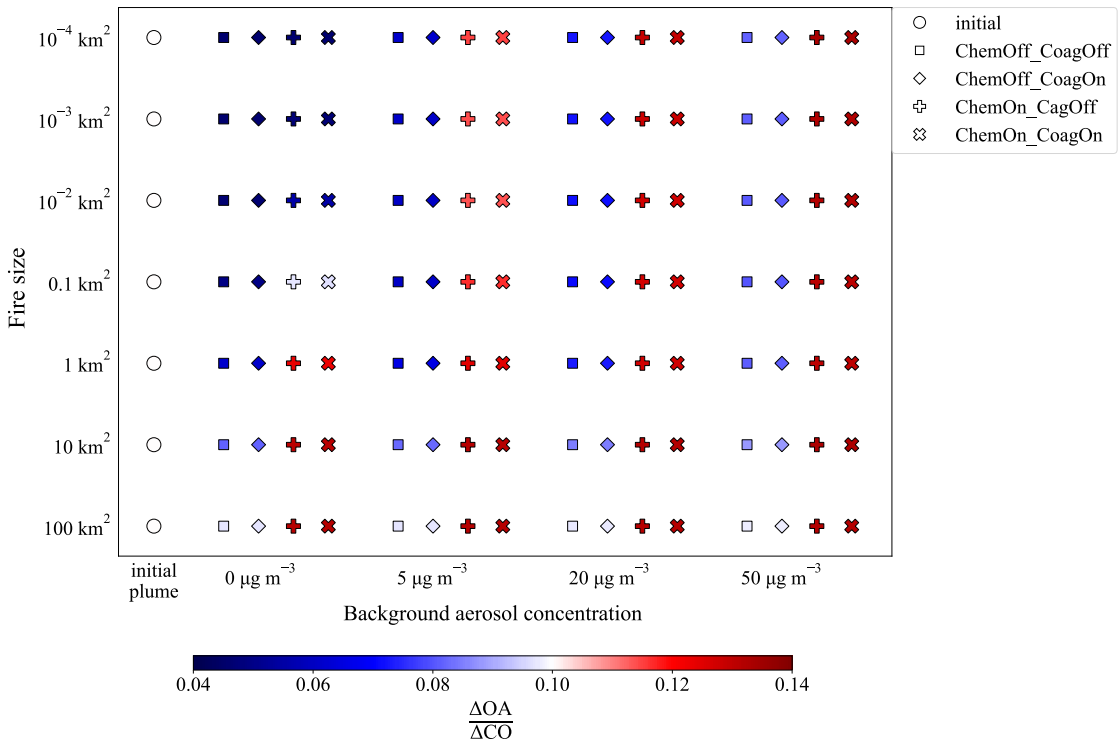

Figure S3. The in-plume normalized organic aerosol mass enhancement (ΔOA/ΔCO) initially and after 4 hours of aging for the ChemOff and ChemOn base cases (Table 1) for all fire sizes and background concentrations modelled. Warm colors indicate an increase in ΔOA/ΔCO after 4 hours of aging, and cool colors represent a decrease. The y axis represents fire size/dilution rate; the x axis represents the background aerosol concentration.

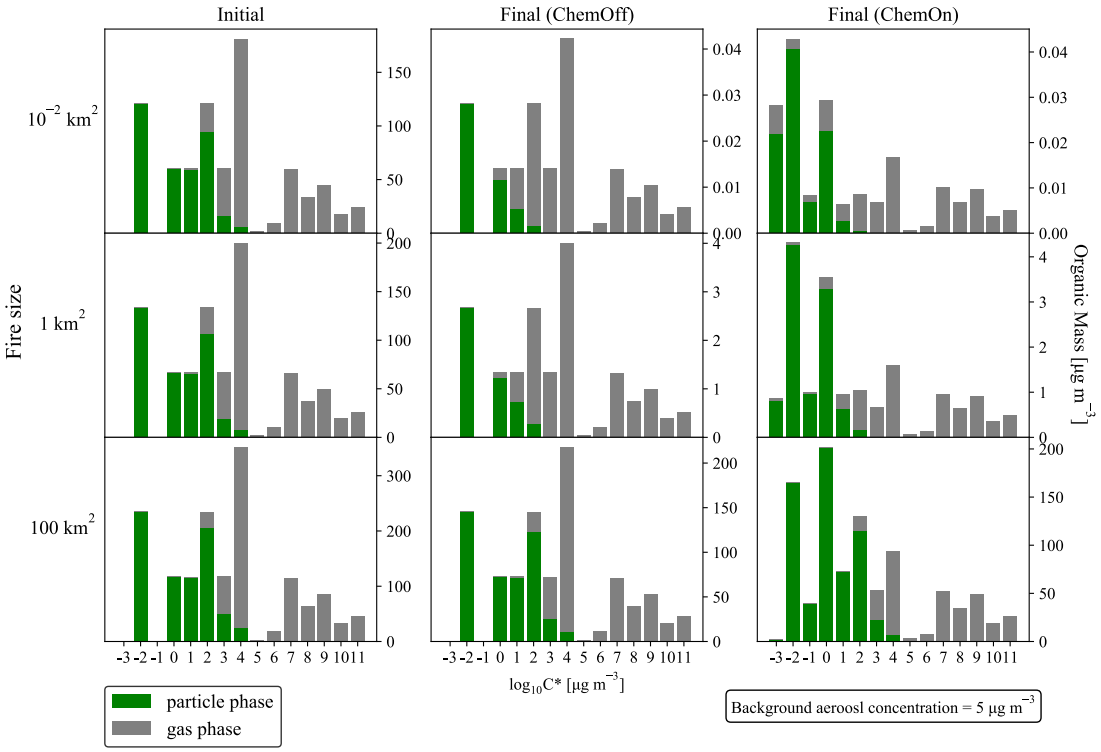

Figure S4. Initial (first column) and final (after 4 hours of aging) VBS distributions for the ChemOff (second column) and ChemOn (third column) base simulations for a background aerosol concentration of 5 μg m^{-3}. Particle phase loadings are in green and gas phase loadings are in grey (all in μg m^{-1}). We use the CoagOn version of each ChemOff/ChemOn case. Shown are fire sizes 10^{-2} km^2 (top row), 1 km^2 (second row), and 100 km^2 (bottom row). The highest volatility bins undergo very little aging as only a small fraction of the material in these bins oxidizes under the k_{OH} parameterization used.

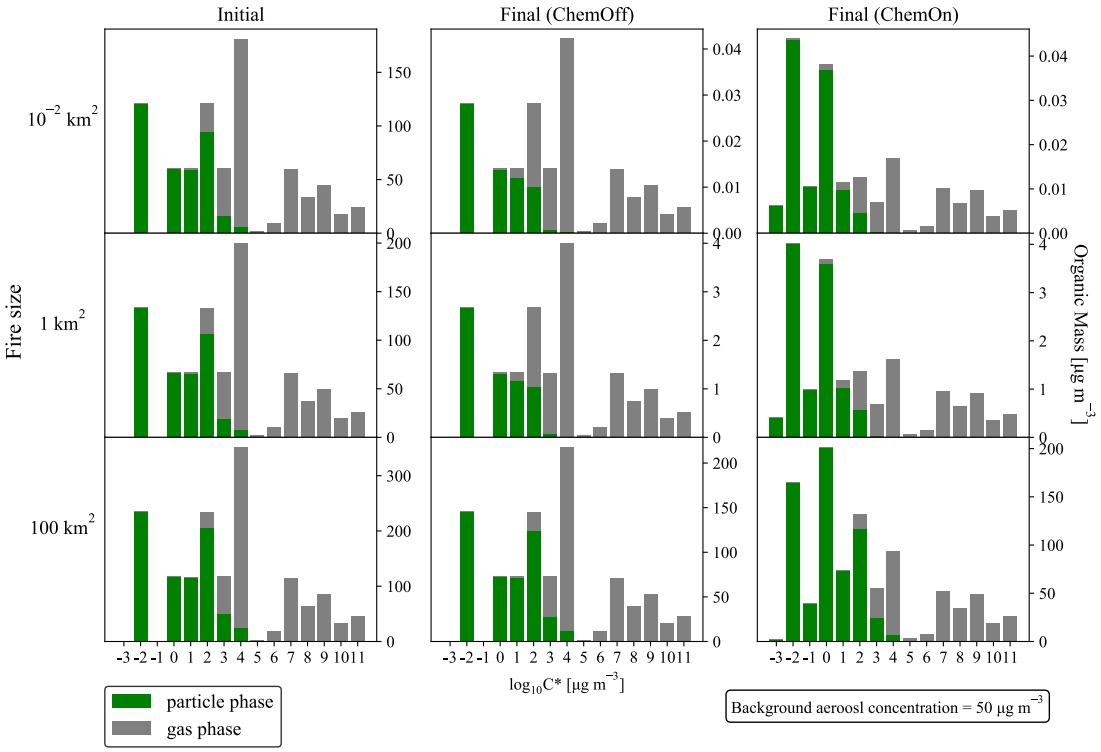

Figure S5. Initial (first column) and final (after 4 hours of aging) VBS distributions for the ChemOff (second column) and ChemOn (third column) base simulations for a background aerosol concentration of 50 μg m^{-3}. Particle phase loadings are in green and gas phase loadings are in grey (all in μg m^{-1}). We use the CoagOn version of each ChemOff/ChemOn case. Shown are fire sizes 10^{-2} km^2 (top row), 1 km^2 (second row), and 100 km^2 (bottom row). The highest volatility bins undergo very little aging as only a small fraction of the material in these bins oxidizes under the k_{OH} parameterization used.

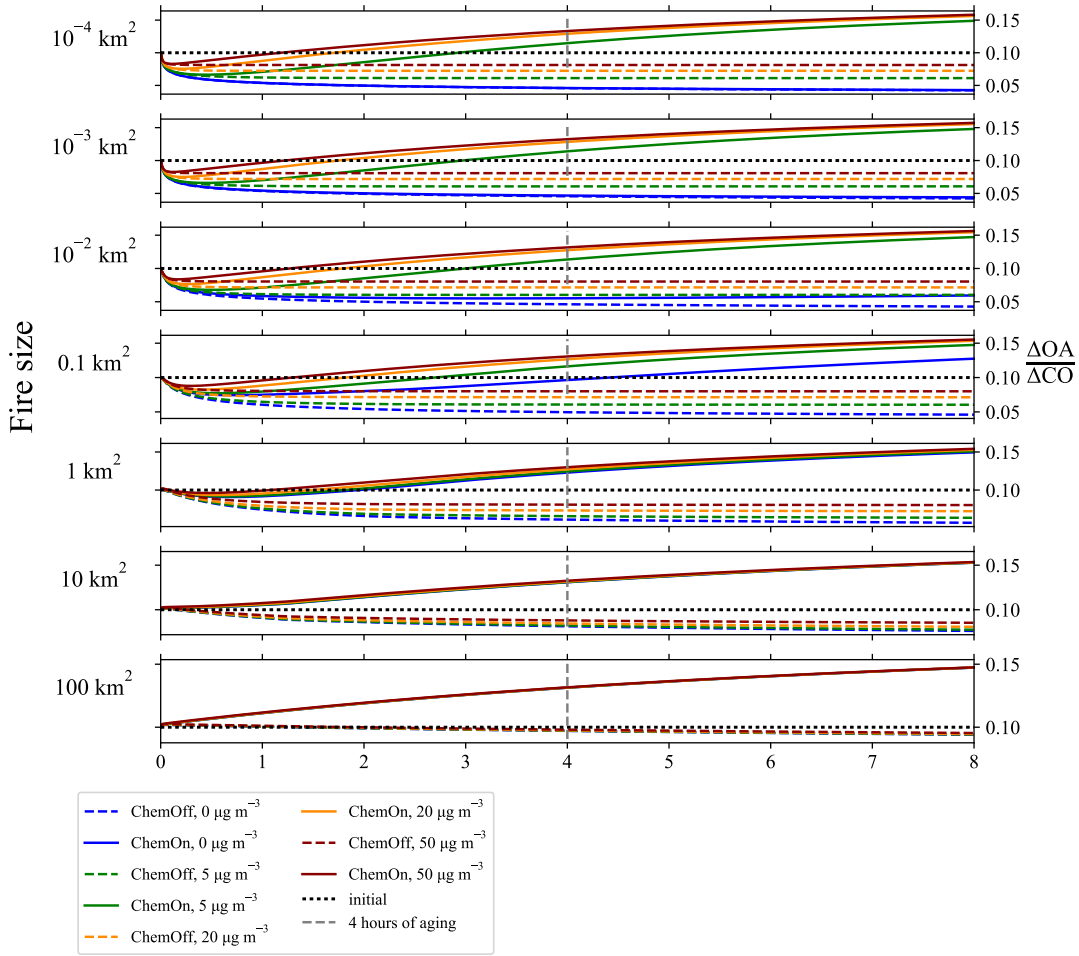

Figure S6. ΔOA/ΔCO for the base cases (Table 1). The vertical grey dashed line is set to 4 hours to guide the eye, as the majority of analyses in this study is done for 4 hours of aging in the model. The initial line in each plot is also to guide the eye: cases that go above the initial line indicate a net normalized gain in mass and cases that go below the initial line indicate a net normalized loss in mass.

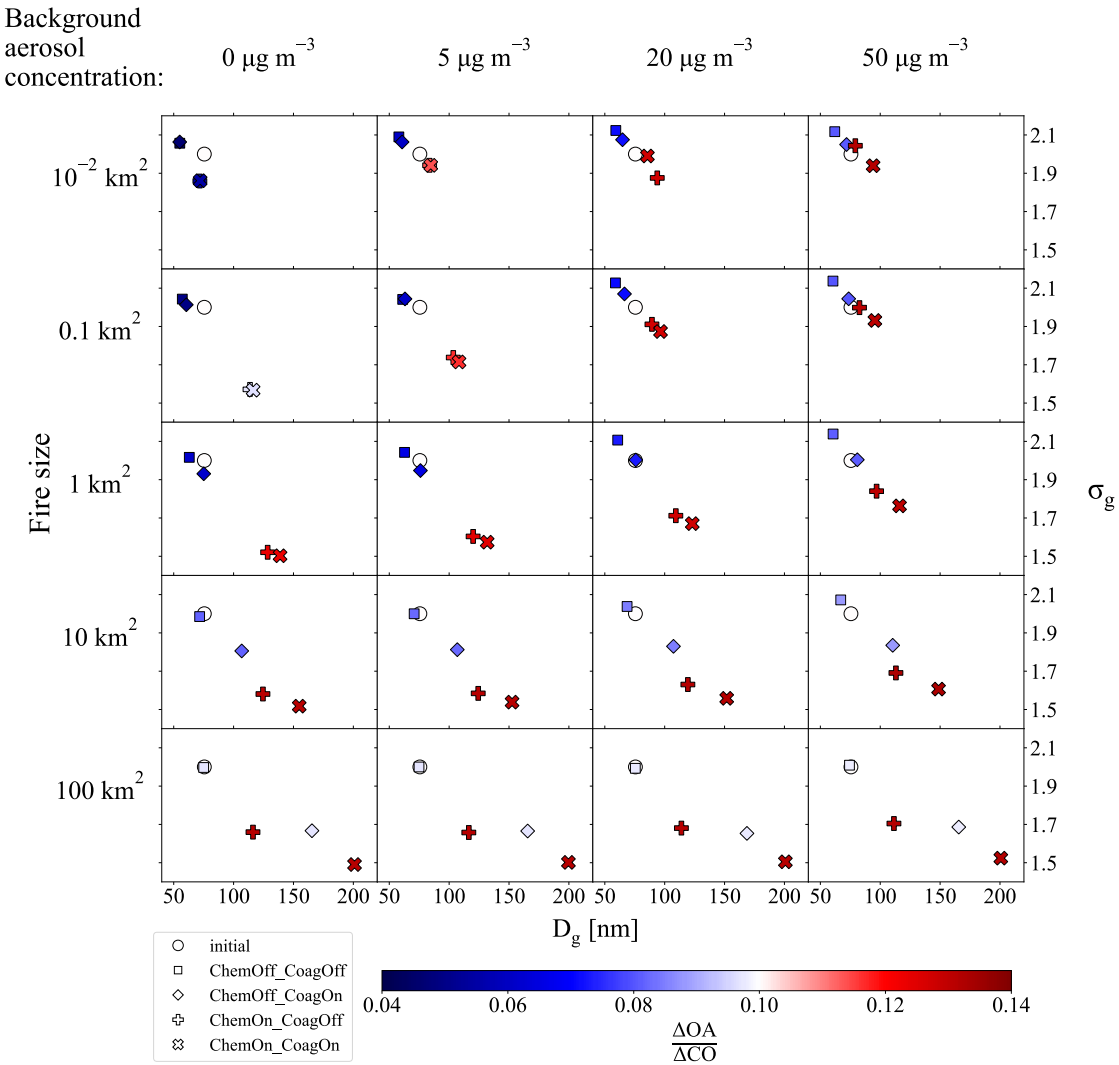

Figure S7. Smoke (background corrected) lognormal median diameter of the lognormal mode (D_g; x axis) and lognormal modal width (σ_g; y axis) after 4 hours of aging for the base cases (Table 1) for all fire sizes between 10^{-2}-100 km^2 and all background aerosol concentrations modelled.. The colorbar is ΔOA/ΔCO initially and after 4 hours of aging for the base cases (same colorbar as Fig S2). The ChemOff_CoagOn case for the 10^{-2} km^2 fire with a 20 μg m^{-3} background was removed due to model noise; for more detail, see Sect. S2.

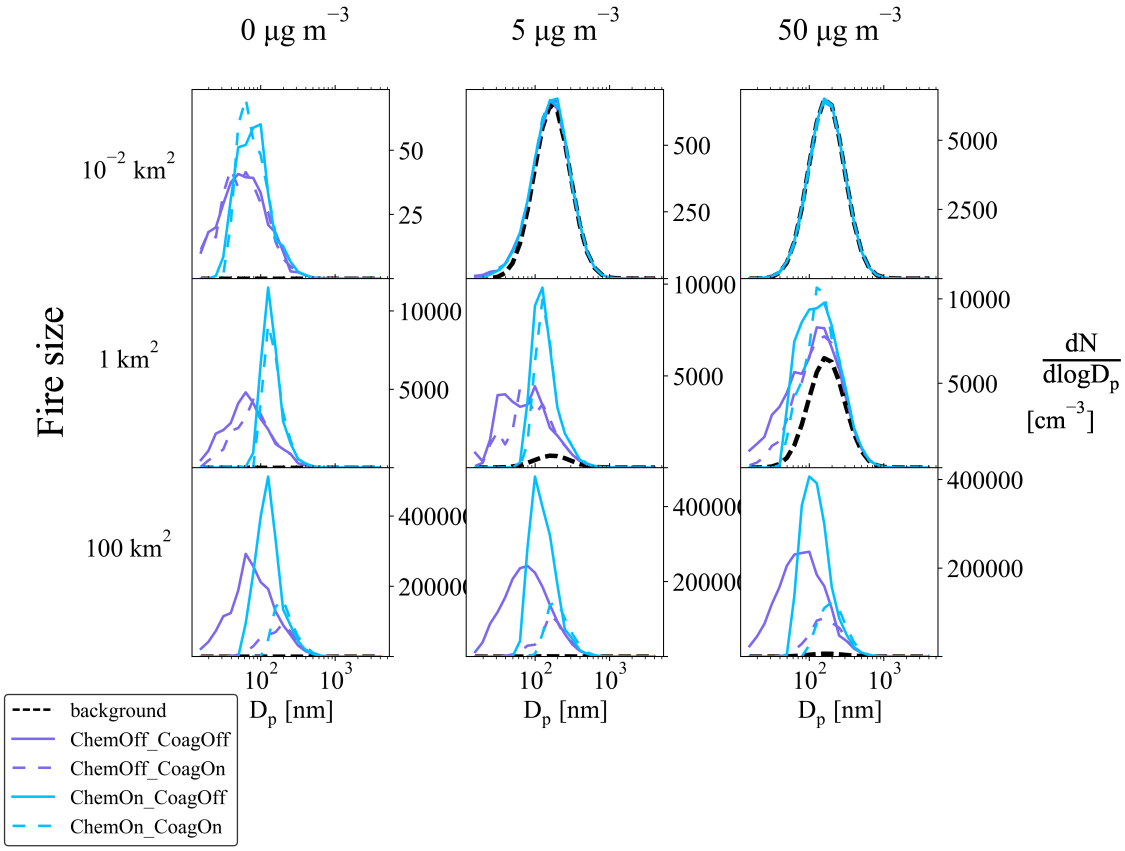

Figure S8. Final number size distributions for the base cases (Table 1) after 4 hours of aging. Shown are 10^{-2} km^2 (top row), 1 km^2 (middle row), and 100 km^2 (bottom row)-sized fires with background concentrations of 0 (first column), 5 (second column), and 50 (final column) μg m^{-3}. The colored lines show the combined plume and background size distributions; the black dashed line shows the background alone. The 100 km^2 fires are large enough above background that the background distribution appears close to zero. The 10^{-2} km^2 fire dilutes and evaporates down to essentially the background distribution for the 50 μg m^{-3} case. The distributions were smoothed as described in Sect. S2.

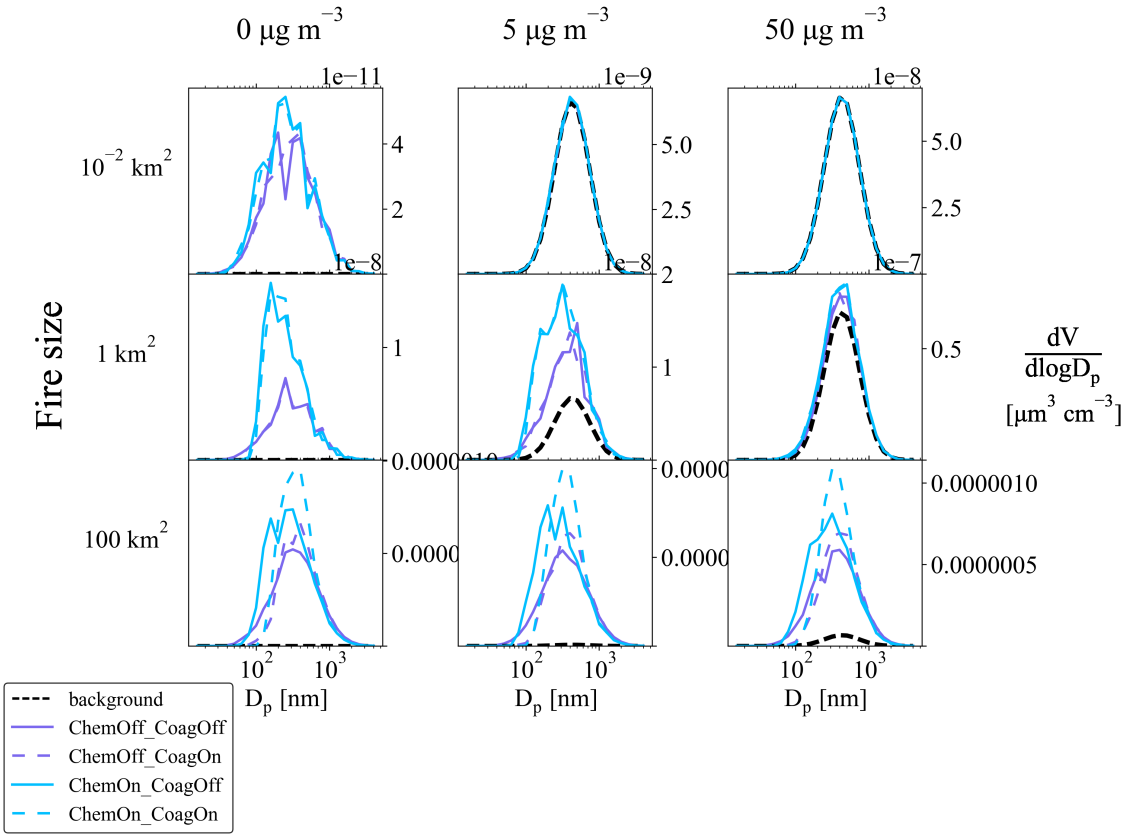

Figure S9. Final volume size distributions for the base cases (Table 1) after 4 hours of aging. Shown are 10^{-2} km^2 (top row), 1 km^2 (middle row), and 100 km^2 (bottom row)-sized fires with background concentrations of 0 (first column), 5 (second column), and 50 (final column) μg m^{-3}. The colored lines show the combined plume and background size distributions; the black dashed line shows the background alone. The 100 km^2 fires are large enough above background that the background distribution appears close to zero. The 10^{-2} km^2 fire dilutes and evaporates down to essentially the background distribution for the 50 μg m^{-3} case. The distributions were smoothed as described in Sect. S2.

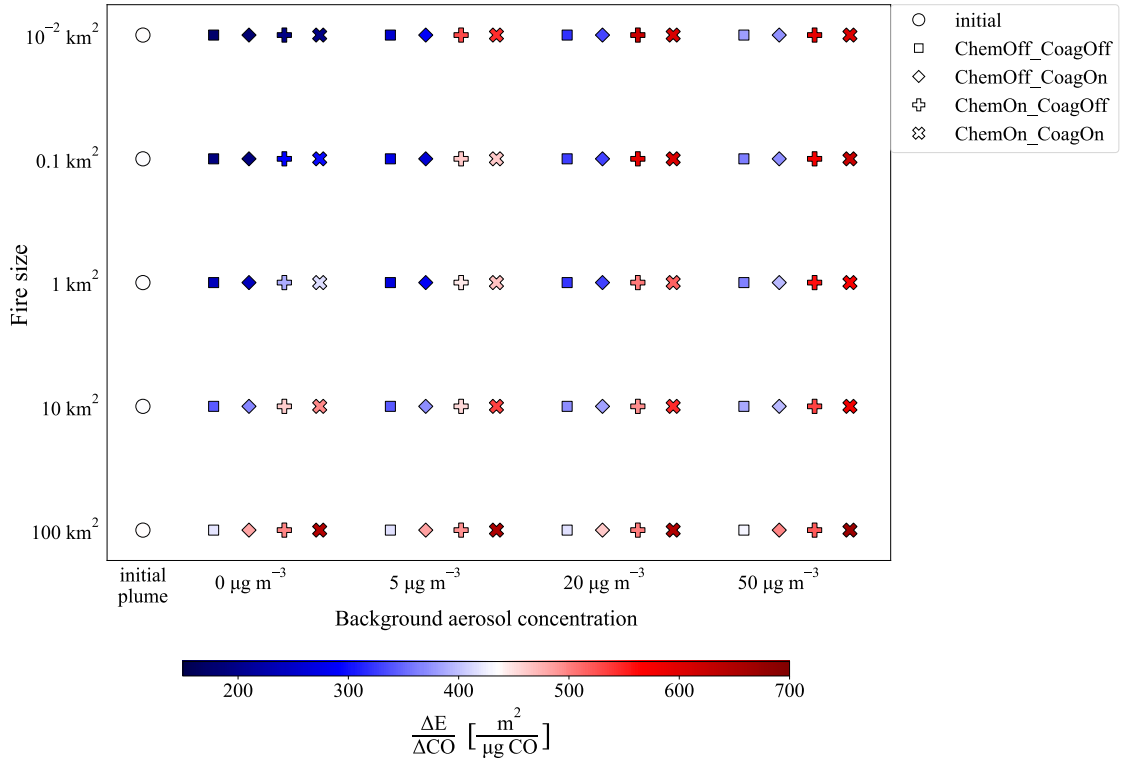

Figure S10. The normalized extinction efficiency ($\Delta E/\Delta \mathrm{CO}$) initially and after 4 hours of aging for the primary cases (Table 1) for all fire sizes between 10^{-2}-100 km^2 and all background aerosol concentrations modelled. For this study, we assume spherical particles with a refractive index of 1.5 - 0.08i at a wavelength of 500 nm. Warm colors indicate an increase in the normalized values while cool colors represent a decrease.The y axis represents fire size/dilution rate; the x axis represents the background aerosol concentration.

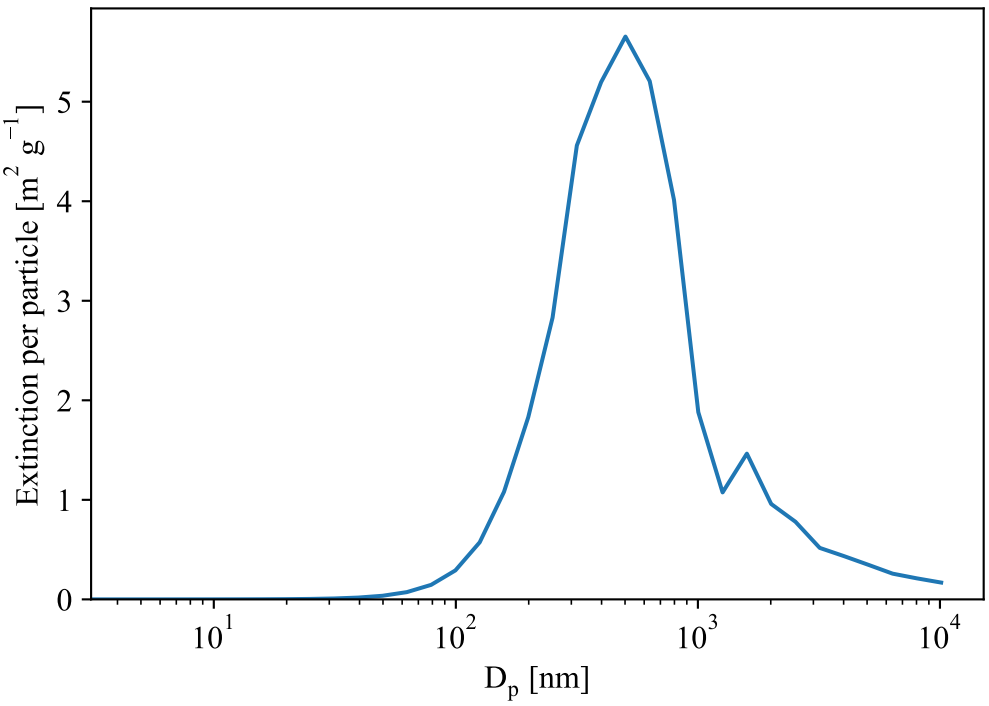

Figure S11. Size dependent mass extinction efficiency for a refractive index of 1.5 - 0.08*i* (assuming spherical particles) at a wavelength of 500 nm. The peak scattering efficiency is at ~500 nm.

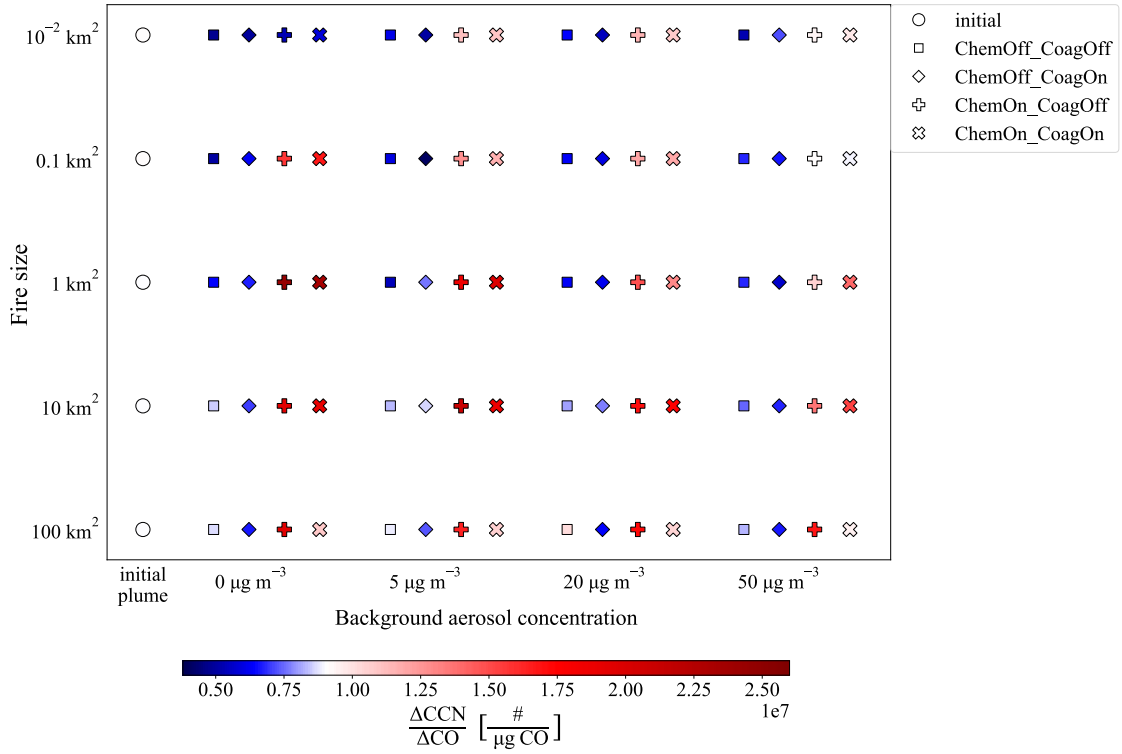

Figure S12. The normalized CCN (ΔCCN/ΔCO) initially and after 4 hours of aging for the primary cases (Table 1) for all fire sizes between 10^{-2}-100 km^2 and all background aerosol concentrations modelled. For this study, we assume spherical particles with a refractive index of 1.5 - 0.08*i* at a wavelength of 500 nm. Warm colors indicate an increase in the normalized values while cool colors represent a decrease.The y axis represents fire size/dilution rate; the x axis represents the background aerosol concentration.

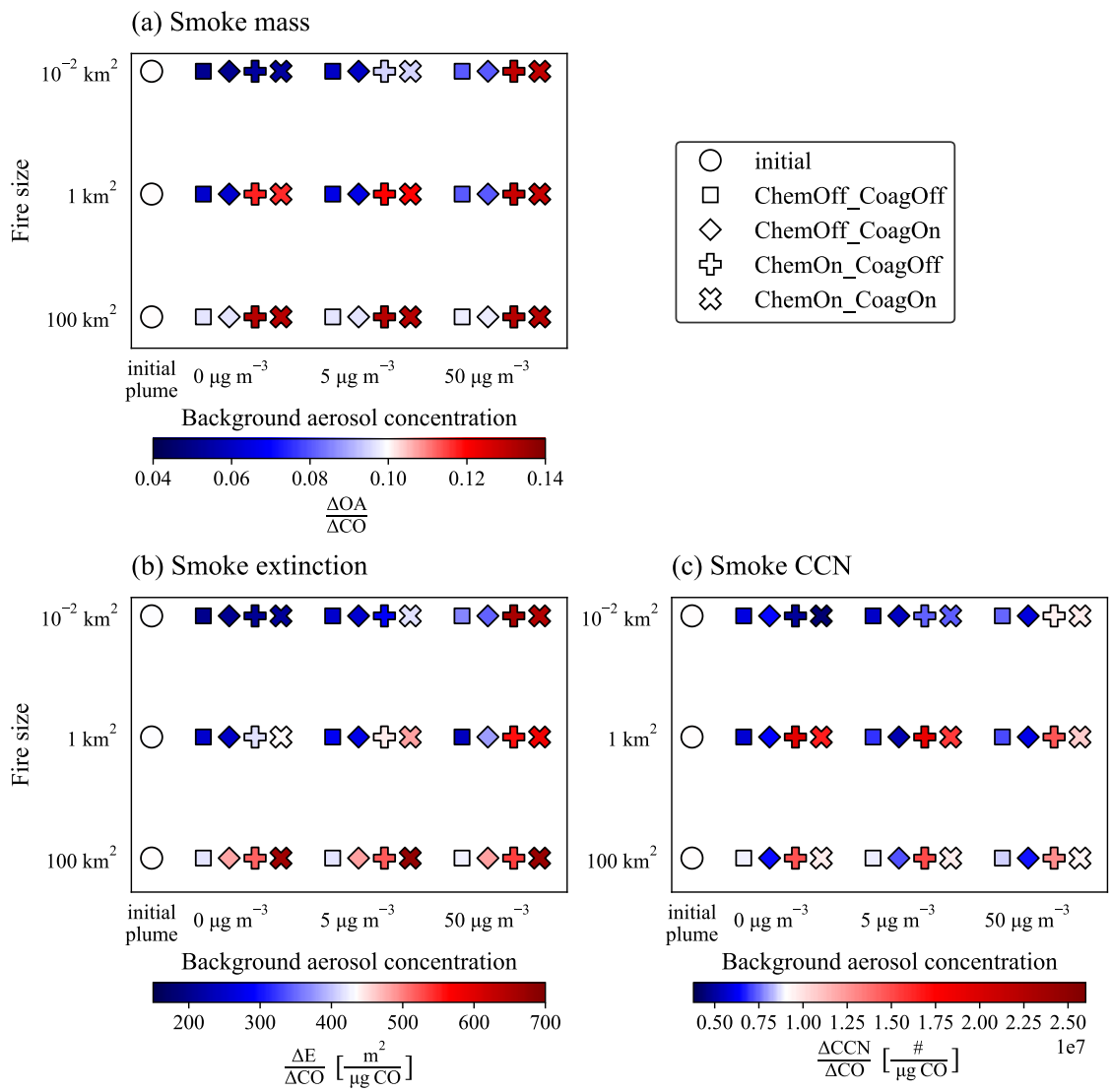

Figure S13. Sensitivity case: accommodation coefficient (α) of 0.1. (a) The in-plume normalized organic aerosol mass enhancement (ΔOA/ΔCO) initially and after 4 hours of aging. (b) The normalized extinction efficiency ($\Delta E/\Delta$CO) initially and after 4 hours of aging. (c) The normalized CCN (ΔCCN/ΔCO) from smoke aerosol at 0.2% supersaturation initially and after 4 hours of aging. Warm colors indicate an increase in the normalized values while cool colors represent a decrease.

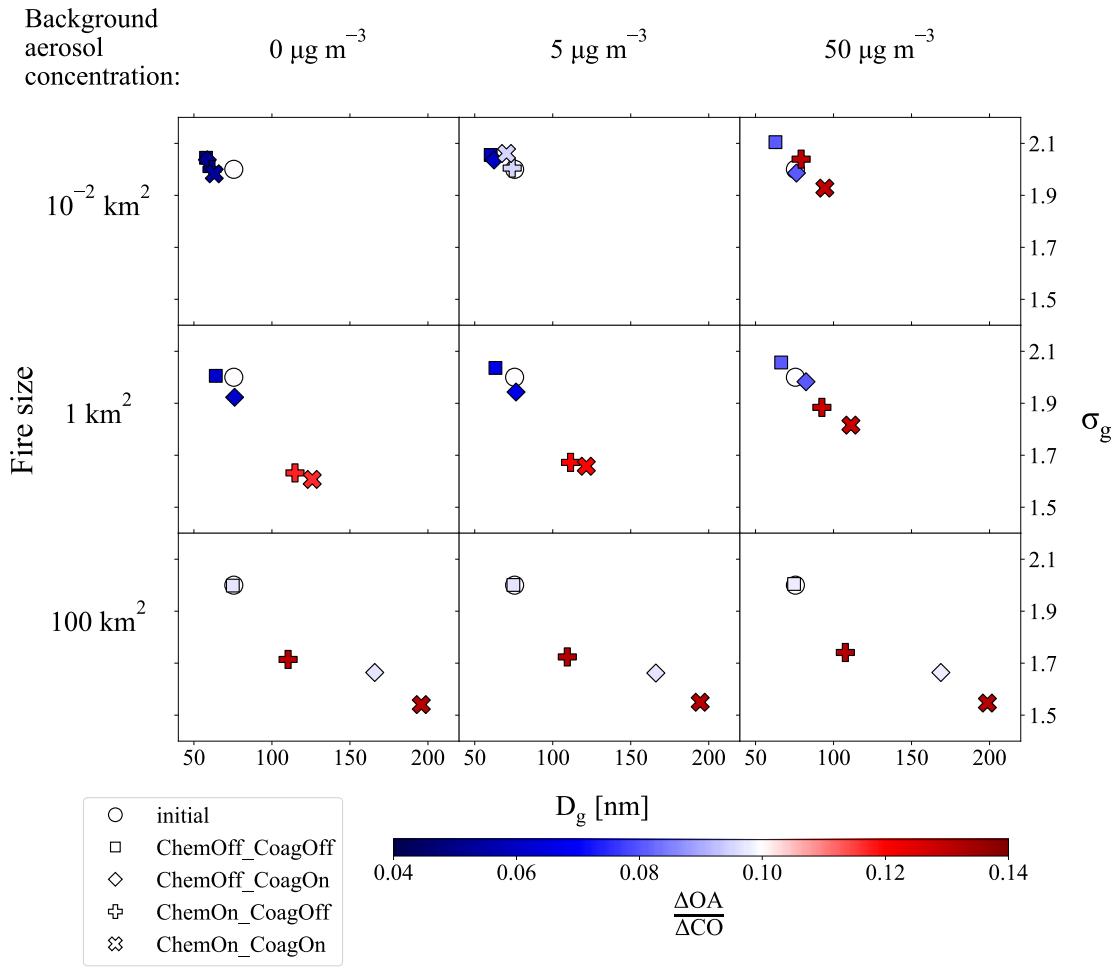

Figure S14. Sensitivity case: accommodation coefficient (α) of 0.1. Smoke (background corrected) lognormal median diameter of the lognormal mode (D_g; x axis) and lognormal modal width (σ_g; y axis) initially and after 4 hours. The colorbar is ΔOA/ΔCO initially and after 4 hours of aging for the base cases (same colorbar as Fig. S12).

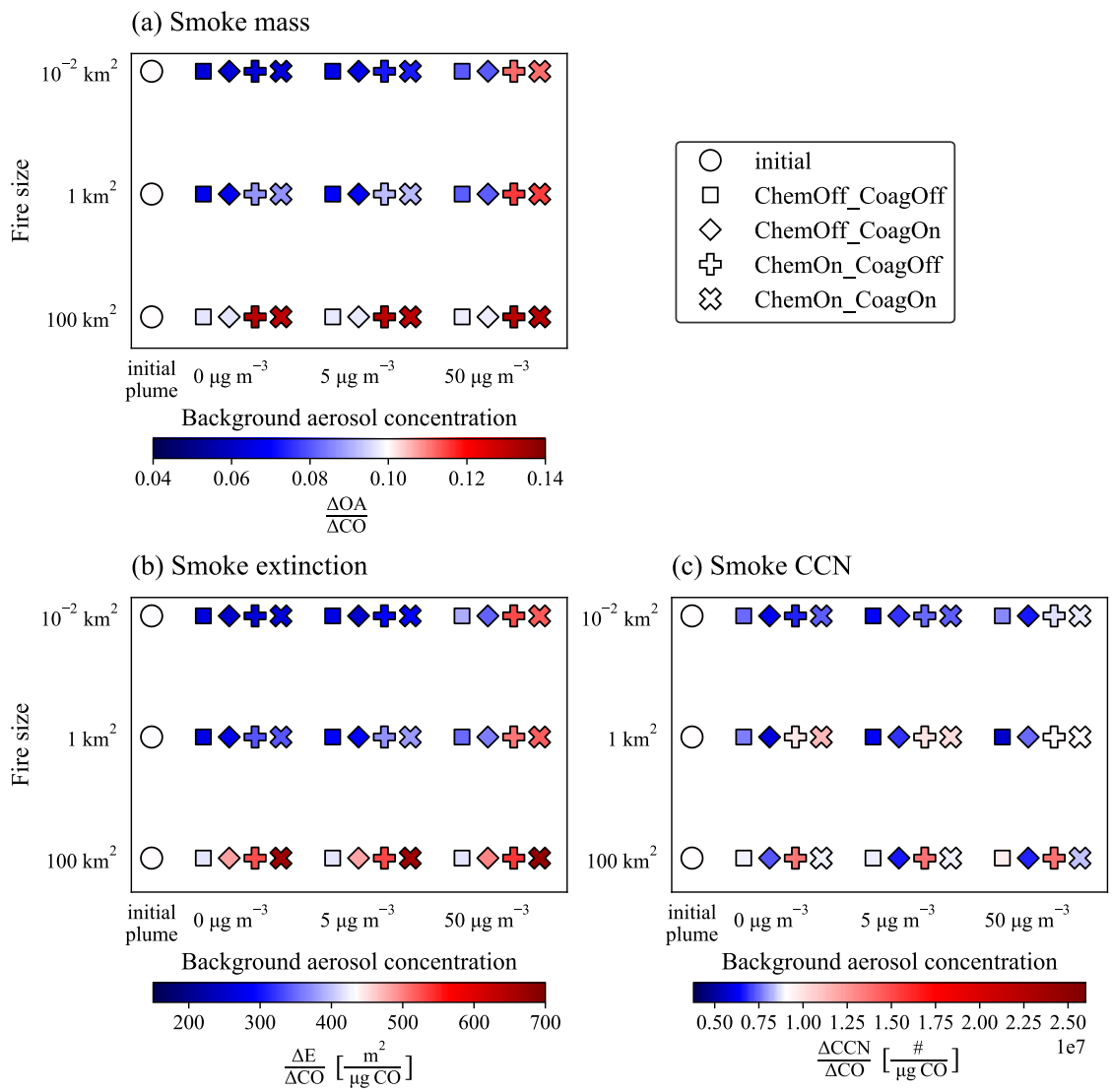

Figure S15. Sensitivity case: accommodation coefficient (α) of 0.01. (a) The in-plume normalized organic aerosol mass enhancement (ΔOA/ΔCO) initially and after 4 hours of aging. (b) The normalized extinction efficiency (ΔE/ΔCO) initially and after 4 hours of aging. (c) The normalized CCN (ΔCCN/ΔCO) from smoke aerosol at 0.2% supersaturation initially and after 4 hours of aging. Warm colors indicate an increase in the normalized values while cool colors represent a decrease.

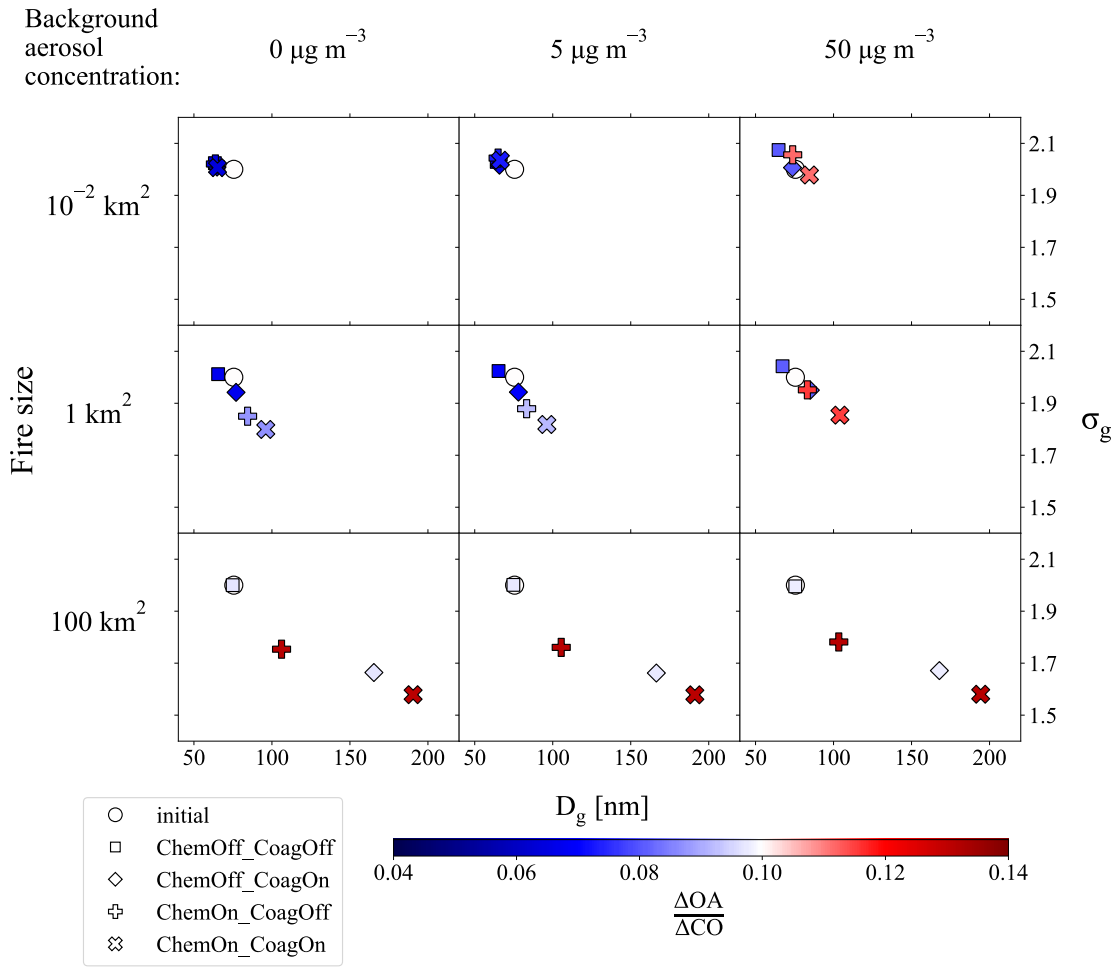

Figure S16. Sensitivity case: accommodation coefficient (α) of 0.01. Smoke (background corrected) lognormal median diameter of the lognormal mode (D_g; x axis) and lognormal modal width (σ_g; y axis) initially and after 4 hours. The colorbar is ΔOA/ΔCO initially and after 4 hours of aging for the base cases (same colorbar as Fig. S14).

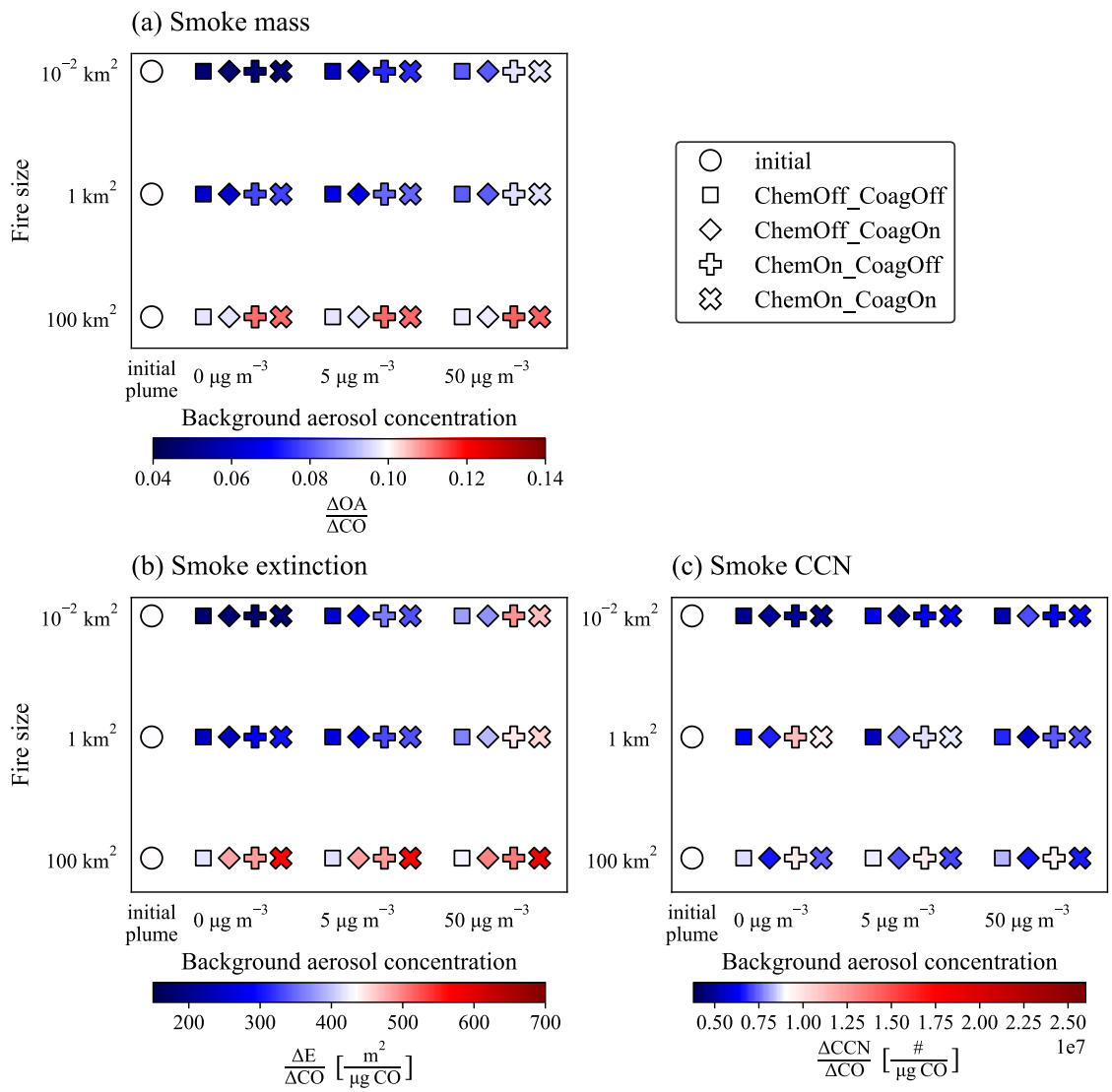

Figure S17. Sensitivity case: chemical production rate, using the rate of reaction with alkanes (Jathar et al., 2014) and a two-bin volatility drop. (a) The in-plume normalized organic aerosol mass enhancement (ΔOA/ΔCO) initially and after 4 hours of aging. (b) The normalized extinction efficiency ($\Delta E/\Delta$CO) initially and after 4 hours of aging. (c) The normalized CCN (ΔCCN/ΔCO) from smoke aerosol at 0.2% supersaturation initially and after 4 hours of aging. Warm colors indicate an increase in the normalized values while cool colors represent a decrease.

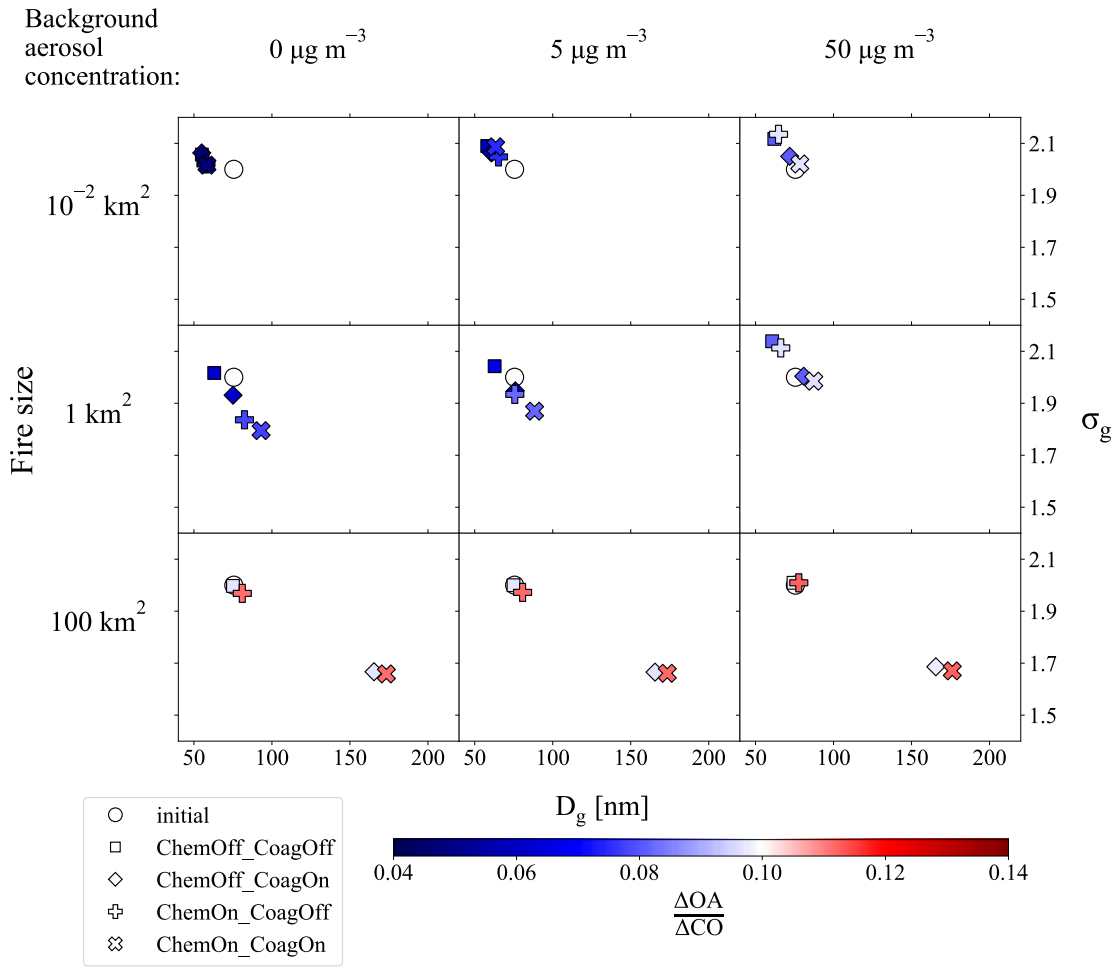

Figure S18. Sensitivity case: chemical production rate, using the rate of reaction with alkanes (Jathar et al., 2014) and a two-bin volatility drop. Smoke (background corrected) lognormal median diameter of the lognormal mode (D_g; x axis) and lognormal modal width (σ_g; y axis) initially and after 4 hours. The colorbar is ΔOA/ΔCO initially and after 4 hours of aging for the base cases (same colorbar as Fig. S16).

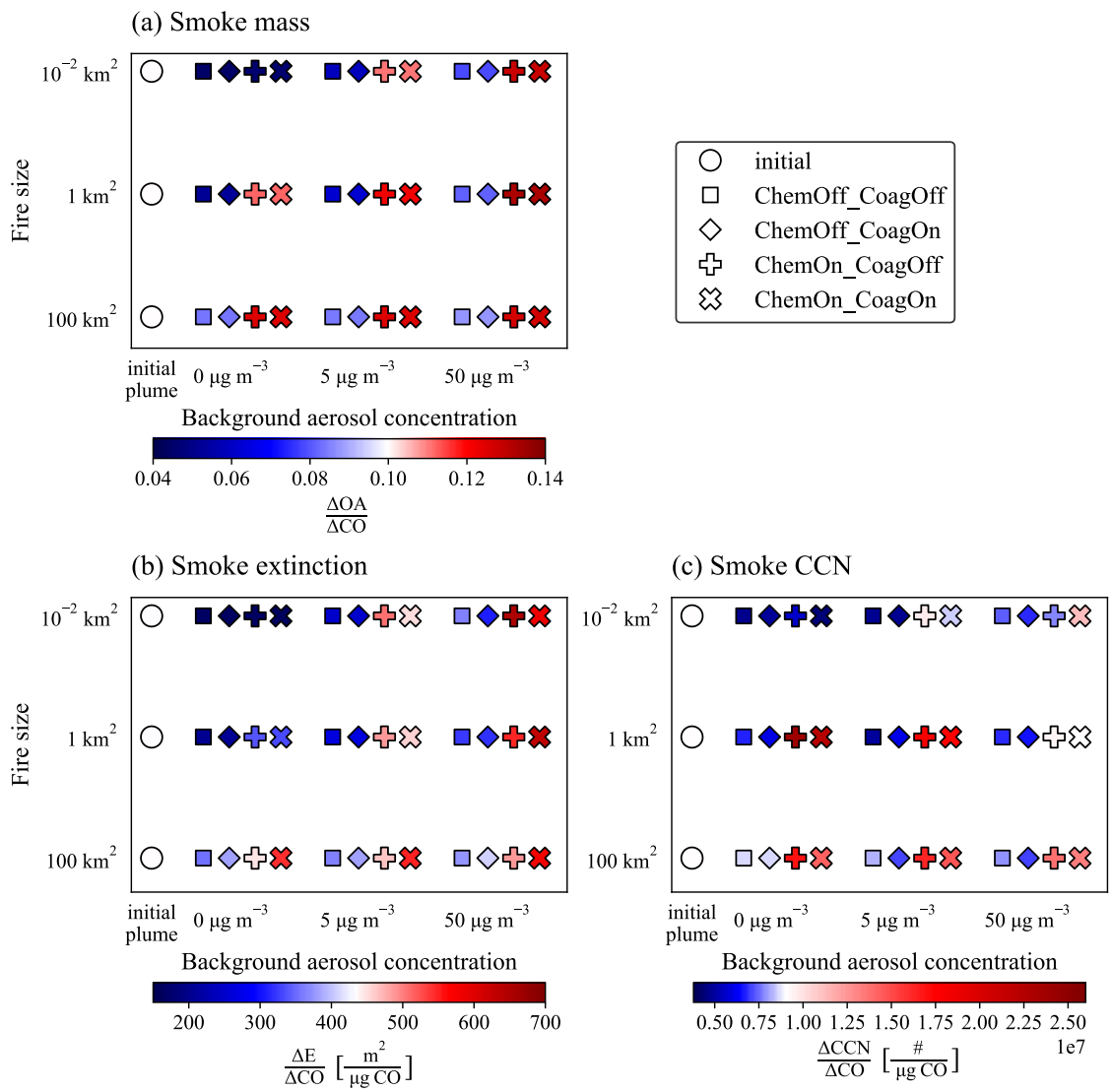

Figure S19. Sensitivity case: stability class of B. (a) The in-plume normalized organic aerosol mass enhancement (ΔOA/ΔCO) initially and after 4 hours of aging. (b) The normalized extinction efficiency ($\Delta E/\Delta$CO) initially and after 4 hours of aging. (c) The normalized CCN (ΔCCN/ΔCO) from smoke aerosol at 0.2% supersaturation initially and after 4 hours of aging. Warm colors indicate an increase in the normalized values while cool colors represent a decrease.The value for the ChemOn_CoagOFF case for E_{smoke} for the 10^{-2} fire size with a 50 μg m^{-3} background concentration has been removed due to model noise; see Sect. S2 for more details.

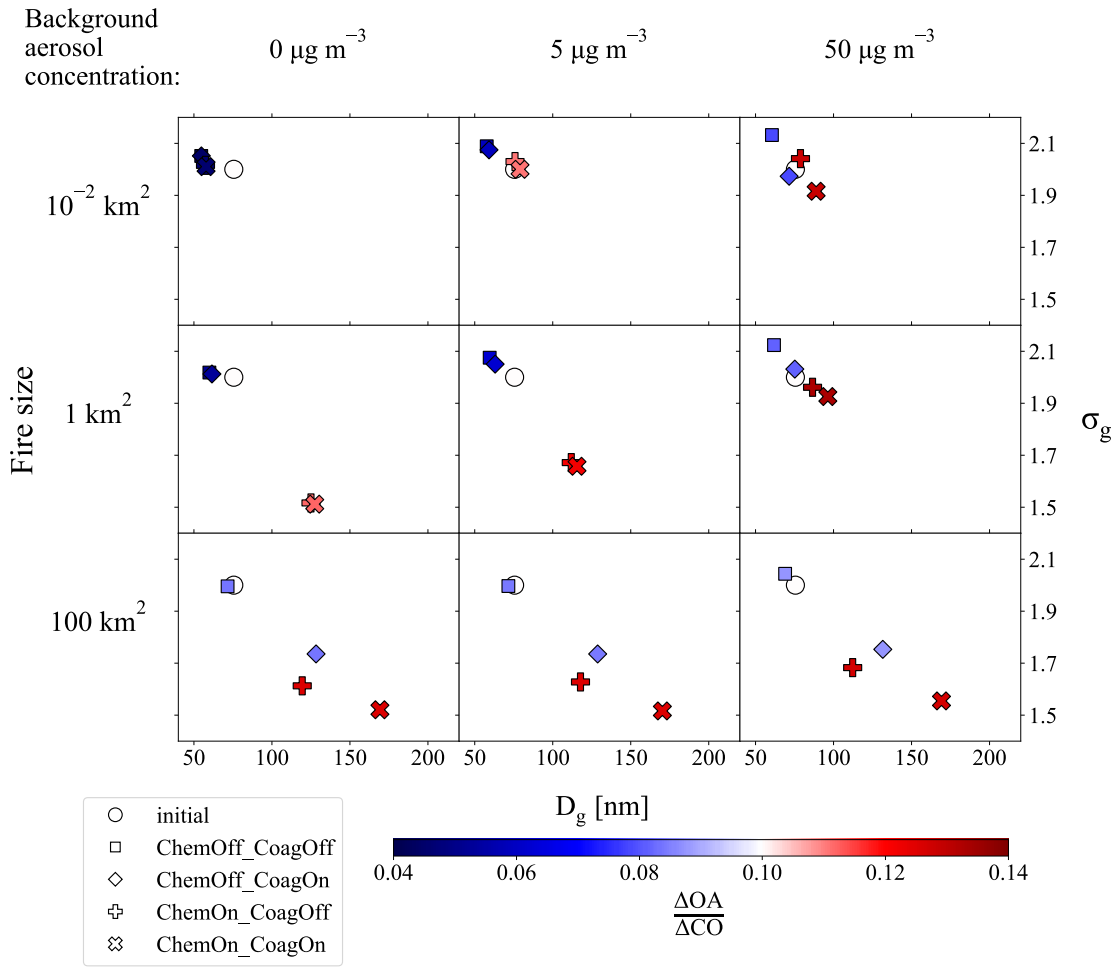

Figure S20. Sensitivity case: stability class of B. Smoke (background corrected) lognormal median diameter of the lognormal mode (D_g; x axis) and lognormal modal width (σ_g; y axis) initially and after 4 hours. The colorbar is ΔOA/ΔCO initially and after 4 hours of aging for the base cases (same colorbar as Fig. S18).

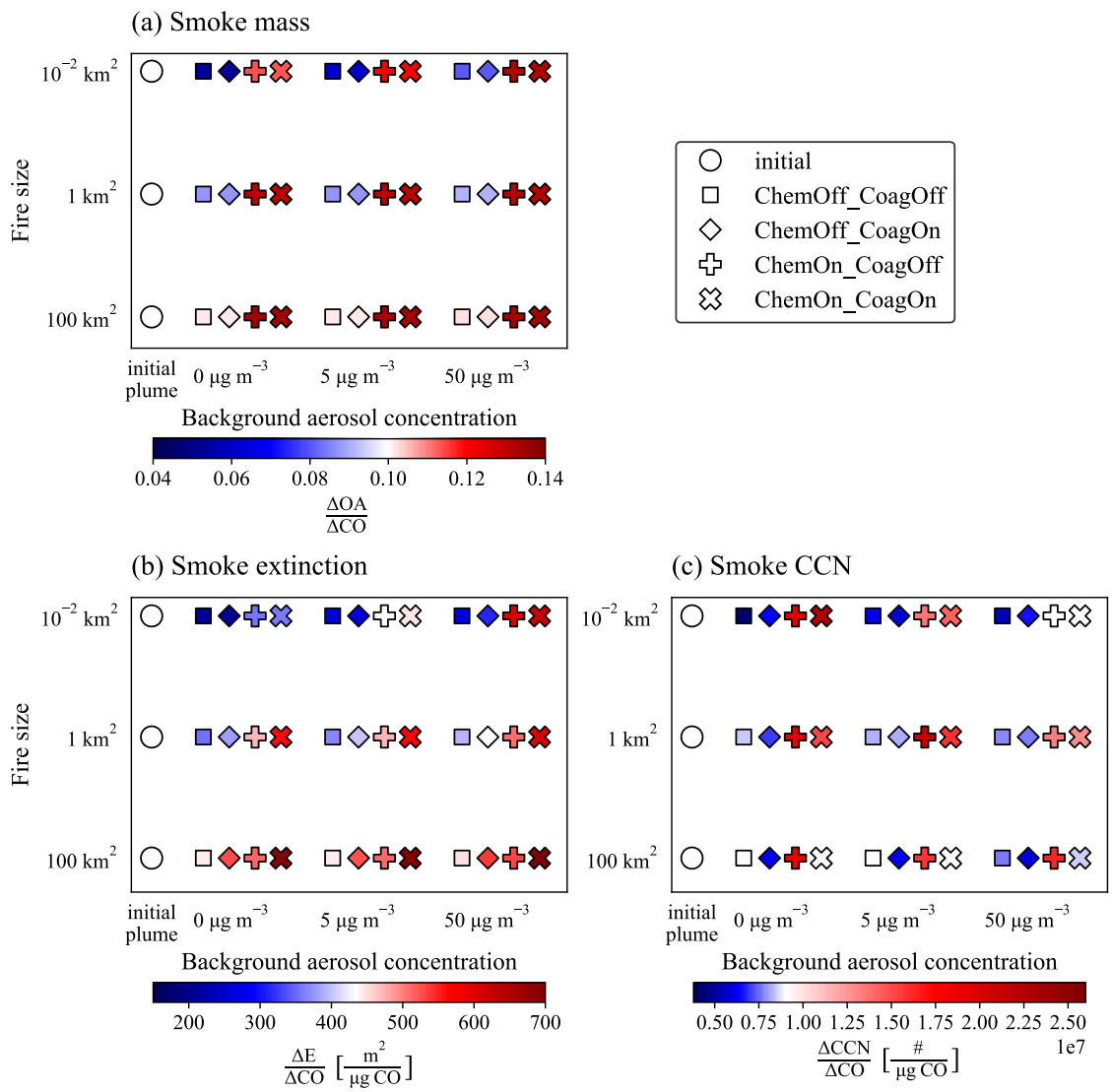

Figure S21. Sensitivity case: stability class of F. (a) The in-plume normalized organic aerosol mass enhancement (ΔOA/ΔCO) initially and after 4 hours of aging. (b) The normalized extinction efficiency ($\Delta E/\Delta$CO) initially and after 4 hours of aging. (c) The normalized CCN (ΔCCN/ΔCO) from smoke aerosol at 0.2% supersaturation initially and after 4 hours of aging. Warm colors indicate an increase in the normalized values while cool colors represent a decrease.

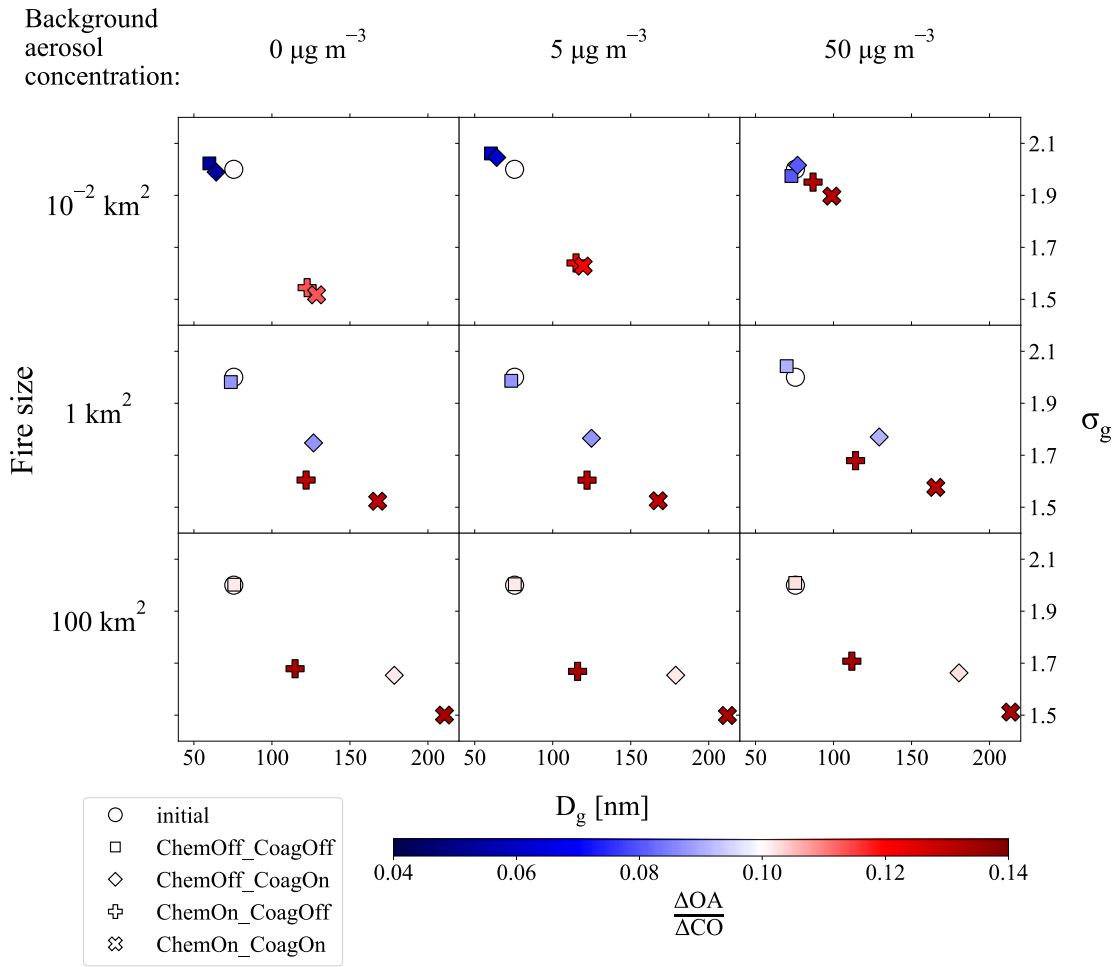

Figure S22. Sensitivity case: stability class of F. Smoke (background corrected) lognormal median diameter of the lognormal mode (D_g; x axis) and lognormal modal width (σ_g; y axis) initially and after 4 hours. The colorbar is ΔOA/ΔCO initially and after 4 hours of aging for the base cases (same colorbar as Fig. S20).

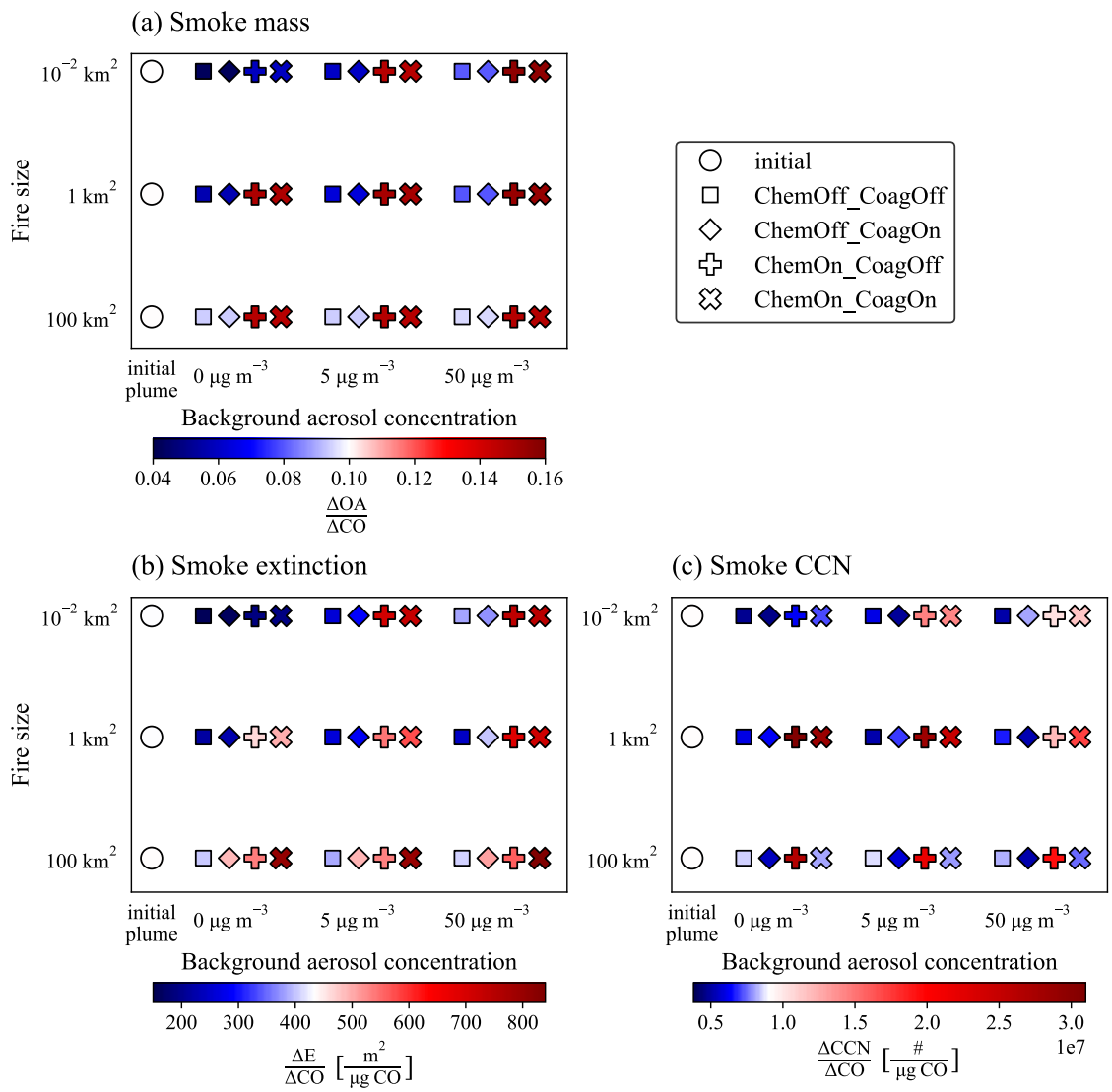

Figure S23. Sensitivity case: aging for 8 hours, using the model settings of the primary cases (Table 1). (a) The in-plume normalized organic aerosol mass enhancement (ΔOA/ΔCO) initially and after 8 hours of aging. (b) The normalized extinction efficiency ($\Delta E/\Delta$CO) initially and after 8 hours of aging. (c) The normalized CCN (ΔCCN/ΔCO) from smoke aerosol at 0.2% supersaturation initially and after 8 hours of aging. Warm colors indicate an increase in the normalized values while cool colors represent a decrease.Note that the maximum of the colorbar for the smoke mass has been increased from 0.14 to 0.16, the maximum of the colorbar for the smoke extinction has been increased from 700 to 840, and the maximum of the colorbar for smoke CCN has been increased from 2.6×10^7 to 3.1×10^7.

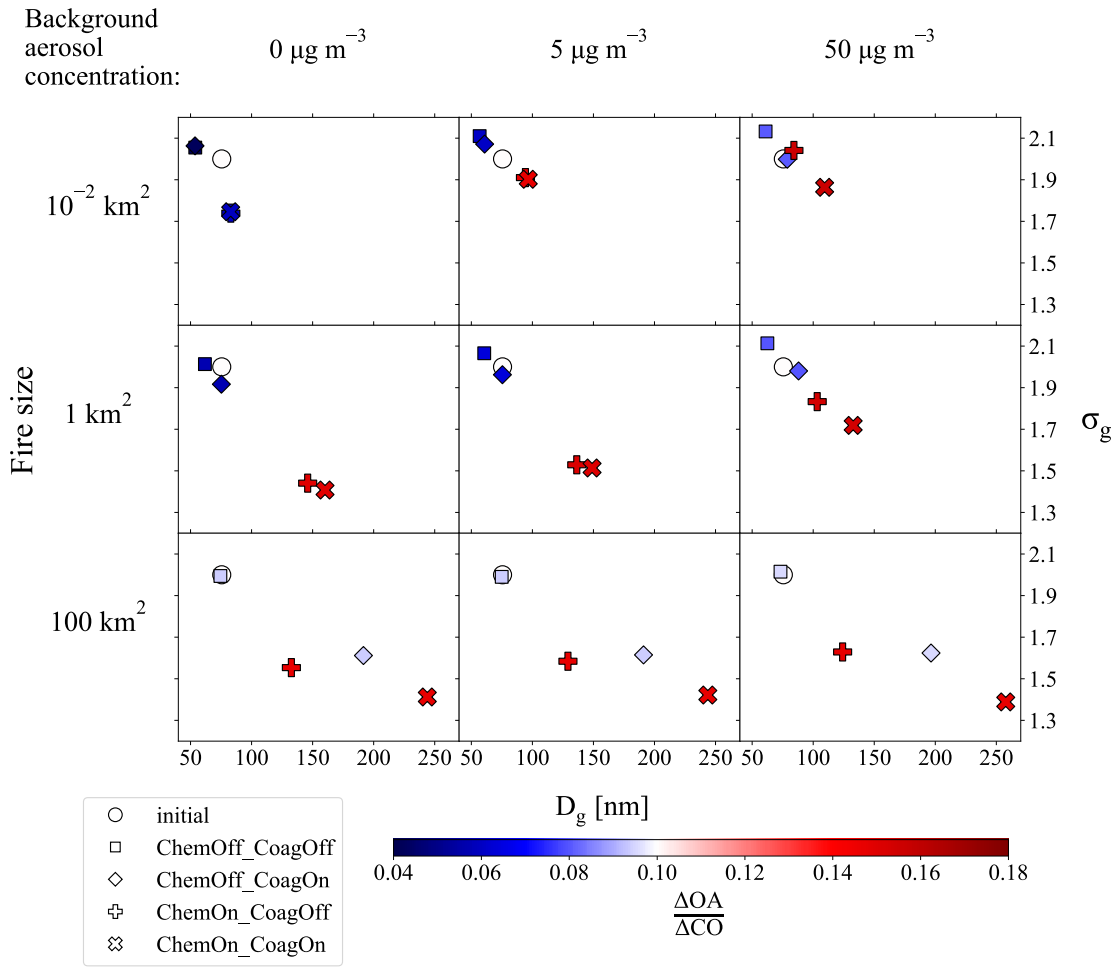

Figure S24. Sensitivity case: aging for 8 hours, using the model settings of the primary cases (Table 1). Smoke (background corrected) lognormal median diameter of the lognormal mode (D_g; x axis) and lognormal modal width (σ_g; y axis) initially and after 8 hours. The colorbar is ΔOA/ΔCO initially and after 4 hours of aging for the base cases (same colorbar as Fig. S22). Note that the maximum of the colorbar for the smoke mass has been increased from 0.14 to 0.16, the x-axis has been increased from 210 to 260 nm, and that the y-axis has been decreased from 1.4 to 1.2..

Table S1. Initial total number concentration for each fire size for the base simulations, as described in Table 1.

Fire size (km^2)	Initial total number concentration (cm^{-3})
100	3.02×10^6
10	1.70×10^5
1	1.61×10^5
10^{-1}	1.52×10^5
10^{-2}	1.44×10^5
10^{-3}	1.36×10^5
10^{-4}	1.29×10^5

Table S2. Details of relevant field campaigns of aging biomass burning measurements. (Uploaded separately.)